Metastable behavior of the superconducting phase in the $BaBi_{1-x}Pb_xO_3$ system

D. T. Marx,* P. G. Radaelli, J. D. Jorgensen, R. L. Hitterman, D. G. Hinks, Shiyou Pei, and B. Dabrowski

Materials Science Division, Argonne National Laboratory, Argonne, Illinois 60439

(Received 4 November 1991; revised manuscript received 24 February 1992)

The structural phases of the $BaBi_{1-x}Pb_xO_3$ system have been studied using neutron powder diffraction. As lead is substituted on the bismuth site, the room-temperature structure is monoclinic for $0.00 \le x \le 0.20$, orthorhombic for $0.25 \le x \le 0.65$, diphasic (orthorhombic and tetragonal) for $0.70 \le x \le 0.80$, and monoclinic for $x = 1.0$. Superconductivity is observed for samples in the composition range $0.70 \le x \le 0.80$. The superconducting phase is the tetragonal phase. *In situ* neutron-powder-diffraction measurements versus temperature show that it is not stable at temperatures below about 425 K. All superconducting samples consist of the metastable tetragonal phase and a semiconducting orthorhombic phase because the tetragonal-to-orthorhombic transition does not proceed to completion. Samples of $Ba_{1-y}K_yBi_{1-x}Pb_xO_3$ have T_c's that are inversely proportional to the total dopant concentration, $x+y$, in the composition region $(0.5 \le x+y \le 0.9)$, where the material is metallic.

INTRODUCTION

Two important oxide superconductors are based on $BaBiO_3$. This parent compound has a body-centered monoclinic structure,[1-4] arising from distortions of the cubic perovskite structure. The monoclinic symmetry results from a rotation of the BiO_6 octahedra around the pseudocubic [110] axis and a symmetric breathing-mode distortion produced by oxygen-atom displacements toward or away from the bismuth atoms. The breathing-mode distortion results in two distinct bismuth sites in each unit cell producing a bond-order charge-density wave (CDW) and giving rise to the observed insulating behavior. Metallic behavior would be expected from simple band-theory arguments because the conduction band is half filled; however, the CDW creates a gap at the Fermi energy resulting in a filled lower band and an empty upper band.[5]

Substituting lead on the bismuth site to form $BaBi_{1-x}Pb_xO_3$ (Ref. 6) produces dramatic changes in the structural and electrical properties. Superconductivity with a maximum T_c of 13 K is observed for $x = 0.70$.[7] In most of the early work, it was concluded that superconductivity was associated with a particular phase and extended over a range of compositions. However, the phase diagram, and the extent of the region of superconducting compositions, has been the subject of considerable controversy, as summarized in Fig. 1. The room-temperature structural phase diagram was investigated by Cox and Sleight[1] using x-ray and neutron powder diffraction. They reported a monoclinic- (*I2/m*, No. 12) to-orthorhombic (*Ibmm*, No. 74) phase transition at $x = 0.10$. Further lead substitution resulted in a tetragonal (*I4/mcm*, No. 140) structure for compositions with $0.65 \le x \le 0.95$. They concluded that compositions with $0.10 \le x \le 0.65$ have orthorhombic symmetry, but the space group was not determined. Kahn *et al.*[8] used x-ray diffraction and concluded that all compositions, $0 \le x \le 1$, in the solid solution are orthorhombic (*Cmm*2, No. 67). Other x-ray- and neutron-diffraction studies[9-11] resulted in reports that samples with $0.70 \le x \le 0.80$ can be either orthorhombic (*Ibmm*) or tetragonal (*I4/mcm*) depending upon the details of the synthesis procedure. Oda *et al.*[10] concluded that both orthorhombic and tetragonal phases are superconducting with $T_c \sim 10$ and 12 K, respectively. From simultaneous refinements using neutron- and synchrotron-x-ray-diffraction data, Ihringer *et al.*[12] and Ritter *et al.*[13] concluded that the symmetry for samples with $0.75 \le x \le 1.0$ is monoclinic (*I2/m*) with only one Bi(Pb) site.

Sleight and Cox[14] reexamined the room-temperature structures of two compositions, $x = 0.725$ and 0.70, using high-resolution synchrotron-x-ray diffraction. They proposed that the confusion about structures in the superconducting region was due to the inability to produce

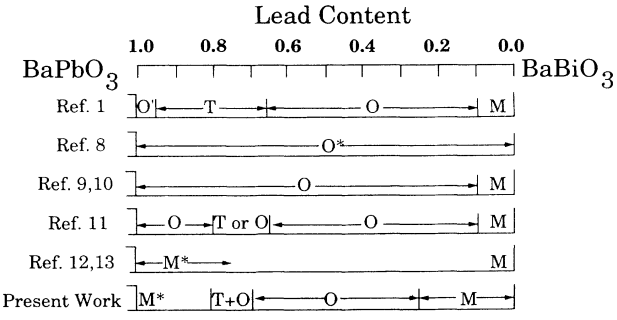

FIG. 1. Room-temperature structures of the $BaBi_{1-x}Pb_xO_3$ system reported in the references indicated. The letters in the phase diagram represent the following structures: *M*, monoclinic (*I2/m* with two inequivalent bismuth sites); *M**, monoclinic (*I2/m* with one Bi site); *O*, orthorhombic (*Ibmm*); *O**, orthorhombic (*Cmm*2); *O'*, orthorhombic (undetermined space group); and *T*, tetragonal (*I4/mcm*).

single-phase samples. They observed the $x=0.70$ sample to be a mixture of a tetragonal phase (50–70%) and an orthorhombic phase (30–50%). Since samples quenched from high temperature were better superconductors than those that had been slowly cooled, they concluded that the tetragonal phase was the superconductor and was stable only at high temperature. However, they did not extend their work to a more detailed study of the high-temperature phase diagram.

Potassium substitution on the barium site of $BaBiO_3$ was recently achieved by Mattheiss, Gyorgy, and Johnson.[15] $Ba_{1-x}K_xBiO_3$ is superconducting with a maximum T_c of 30 K for samples with $x=0.375$.[4,16,17] Work on the structural phase diagram is more definitive than for $BaBi_{1-x}Pb_xO_3$.[4] The room-temperature structures display various distortions of the cubic perovskite structure with only one phase being superconducting. Monoclinic $BaBiO_3$ transforms to an orthorhombic (*Ibmm*, No. 74) structure at $x=0.1$ and to a cubic ($Pm\bar{3}m$, No. 221) structure at $x=0.37$ before reaching the maximum solubility for potassium near $x=0.5$.[4,17] A semiconductor-to-metal transition occurs at the orthorhombic-to-cubic transition. The superconducting phase is the cubic perovskite, with the highest T_c being observed at the phase boundary, where the semiconductor-to-metal transition occurs.

These two oxide superconductors, both based on the same parent phase, display a number of important similarities. In both cases, it appears likely that superconductivity occurs only in one of the several phases that exist as a function of composition. Furthermore, the highest T_c is observed at a phase boundary with a semiconducting phase, suggesting that some form of instability that opens a gap at the Fermi energy limits the maximum T_c that can be obtained. The published data also suggest that the superconducting phases are metastable. In the case of $BaBi_{1-x}Pb_xO_3$, the best superconducting samples are produced by quenching,[14] suggesting that the desired phase is stable only at high temperature. In the case of $Ba_{1-x}K_xBiO_3$, the required level of potassium substitution ($x\geq 0.37$) can only be achieved by a two-step synthesis process in which the potassium is first incorporated at high temperature, where the concentration of oxygen vacancies is high, followed by filling the oxygen vacancies at a lower temperature where decomposition of the compound is prevented by the sluggish kinetics for potassium diffusion.[17,18]

These similarities emphasize the importance of resolving the unanswered questions about the structural phase diagram of the $BaBi_{1-x}Pb_xO_3$ system. The work reported here was undertaken to determine the structure of the superconducting phase and the nature of its metastable behavior. We report a revised room-temperature phase diagram versus composition (included in Fig. 1 for comparison) based on neutron-powder-diffraction studies. We also report temperature-dependent neutron-powder-diffraction studies in which we have observed a structural phase transition from a high-temperature tetragonal to a low-temperature orthorhombic phase. We observe that the phase transition never proceeds to completion. Thus, samples in the composition range $0.70\leq x\leq 0.80$ are diphasic mixtures of tetragonal and orthorhombic phases. The superconducting volume fraction is larger for samples that contain more of the metastable tetragonal phase, leading us to conclude that only the tetragonal phase is superconducting.

SAMPLE PREPARATION AND EXPERIMENTAL PROCEDURE

Powder samples of $BaBi_{1-x}Pb_xO_3$ were prepared over the full composition range, $0\leq x\leq 1$, by solid-state reaction. The starting materials were $BaCO_3$ (99.9997%), Bi_2O_3 (99.996%), and PbO (99.97%). The powders were wet ball milled using *n*-amyl alcohol in an agate jar for 2 h, then dried overnight at 400 K. The dried powder was ball milled for 1 h to ensure uniformity, placed into a gold boat, and fired in flowing ultrahigh-purity oxygen. The maximum firing temperature was varied somewhat with composition to ensure that a full reaction occurred while avoiding melting and loss of lead. Samples were fired at temperatures from 1025 to 1105 K for 12 h followed by slowly cooling (3 K/min) to room temperature. After dry ball milling, the samples were fired a second time using the same procedure.

After it was learned that samples with compositions in the range $0.70\leq x\leq 0.80$ were two-phase mixtures, additional samples of the compositions $x=0.70$, 0.725, 0.75, and 0.80 were prepared by an identical process, except that quenching instead of slow cooling followed each firing. These samples were fired at 1085 K (the same temperature as for the correspondingly slowly cooled samples) for 12 h, and then slowly cooled to 875 K before quenching into liquid nitrogen. The samples were then ball milled for 2 h and a second firing at 1105 K was performed followed by the same cooling and quenching procedure.

Neutron-powder-diffraction experiments were performed at the time-of-flight (TOF) General Purpose Powder Diffractometer at Argonne's Intense Pulsed Neutron Source (IPNS).[19] This instrument achieves resolution of $\Delta d/d\leq 0.025$ for $0.4\leq d\leq 2.8$ Å in backscattering ($2\theta=148°$). The high resolution at large d spacings was advantageous for characterizing the two-phase behavior of some of the samples. For temperatures between 300 and 575 K, a simple radiantly heated furnace was used. A closed-cycle helium refrigerator (Displex) was used to collect data for temperatures between 10 and 300 K. Samples for the low-temperature studies were contained in indium-sealed vanadium cans with 1 atm of He exchange gas at room temperature. For the high-temperature experiments the cans were not sealed. The neutron-powder-diffraction data were analyzed using the TOF Rietveld refinement technique.[20] Only the high-resolution, backscattered data were used in the refinements.

Normal-state and superconducting properties were studied using four-probe dc resistivity and ac susceptibility. Pellets were pressed from previously fired material and refired in flowing oxygen with the maximum firing temperature being determined by the composition as described previously. The pellets were slowly cooled to

room temperature. A uniform bar ($\sim 1\times 1\times 7$ mm^3) was cut from each pellet for dc resistivity measurements for temperatures between 8 and 300 K. Copper leads were attached using conducting silver epoxy. Superconducting transitions were also determined for ground powder samples using a Lakeshore Model 7000 ac susceptometer for temperatures between 5 and 35 K. Data were recorded on warming in a 1-Oe, 100-Hz ac field.

ROOM-TEMPERATURE STRUCTURES OF THE $BaBi_{1-x}Pb_xO_3$ SYSTEM

Neutron-powder-diffraction data for the end-point compounds ($x=0$ and 1) agreed with the previously published structures. $BaBiO_3$ is monoclinic with space group $I2/m$ and has two inequivalent bismuth sites per unit cell.[1-3,21-23] Our refinement results for the present sample agreed with those we have previously published[4] and are not repeated here. $BaPbO_3$ is also monoclinic with space group $I2/m$ but has one bismuth site per unit cell.[13] The monoclinic $BaBiO_3$ and $BaPbO_3$ structures have been compared by Ritter *et al.*[13] Our refined structural parameters for $BaPbO_3$ are presented in Table I and qualitatively agree with those published by Ritter *et al.*[13] However, some atom positions are slightly different and we obtain a monoclinic angle of nearly 90°. These differences lead us to suspect that the space group may not be correct. Since the main focus of this paper is the superconducting composition range, we did not pursue this issue further.

We found the monoclinic $BaBiO_3$ structure to be stable for compositions extending from $x=0$ to $x=0.2$. A portion of the Rietveld refinement profile for a sample with $x=0.10$ is shown in Fig. 2. The monoclinic angle β

TABLE I. Refined structural parameters for $BaPbO_3$ (left) and atomic distances and angles (right) at 295 K. Space group: monoclinic, $I2/m$ (No. 12). The data of the present work are compared with the ones obtained by Ritter *et al.* (Ref. 13). For both sets of data the standard setting (b unique axis) is used.

		This work	Ritter *et al.*		This work	Ritter *et al.*
a (Å)		6.0227(2)	6.0278(1)	Pb-O(1) (Å)	2.1458(5)	2.152(1)
b (Å)		8.5041(1)	8.5109(1)			
c (Å)		6.0617(2)	6.0664(1)	Pb-O(2) (Å)	2.1487(2)	2.157(1)
β		90.006(3)	90.083(2)			
				Pb-O(3) (Å)	2.1477(3)	2.1444(6)
Ba	x	0.247(1)	0.255(1)			
	y	0	0	Ba-O(1) (Å)	2.759(6)	2.73(1)
	z	0.7531(8)	0.751(1)		3.009(8)	2.92(1)
	B (Å^2)	0.71(2)	0.95(2)		3.046(8)	3.14(1)
					3.303(6)	3.34(1)
Pb	x	0.25	0.25			
	y	0.25	0.25	Ba-O(2) (Å)	2.837(4)	2.83(1)
	z	0.25	0.25		3.198(4)	3.22(1)
	B (Å^2)	0.25(1)	0.55(2)			
				Ba-O(3) (Å)	2.861(4)	2.90(1)
O(1)	x	0.2496(8)	0.263(2)		3.175(4)	3.14(1)
	y	0	0			
	z	0.2980(6)	0.301(1)	O(1)-O(2) (Å)	3.018(3)	3.03(1)
	B (Å^2)	1.09(4)	1.4(1)		3.055(3)	3.06(1)
O(2)	x	0	0	O(1)-O(3) (Å)	3.028(3)	3.02(1)
	y	0.2227(2)	0.215(1)		3.044(3)	3.052(1)[a]
	z	0	0			
	B (Å^2)	0.76(3)	1.2(1)	O(2)-O(3) (Å)	3.0114(1)	3.018(1)
					3.0644(5)	3.062(2)
O(3)	x	0	0			
	y	0.2760(3)	0.267(1)	O(3)-O(2)-O(3)	89.97(2)°	90.34(4)°[b]
	z	0.5	0.5			
	B (Å^2)	2.10(5)	1.6(1)	O(1)-Pb-O(2)	90.7(1)°	90.6(3)°
R_{wp} (%)		7.897	13.9	O(1)-Pb-O(3)	90.8(1)°	90.5(3)°
R_{expt} (%)		4.774	9.27			
R_{wp}/R_{expt}		1.654	1.5	O(2)-Pb-O(3)	91.00(1)°	90.9(3)°

[a]A typographical error in Ref. 13 has been corrected by recalculating the distance based on the atomic positions.
[b]This angle is inconsistent with the atomic positions in Ref. 13. The numeric value is in agreement with the angle O(2)-O(3)-O(2).

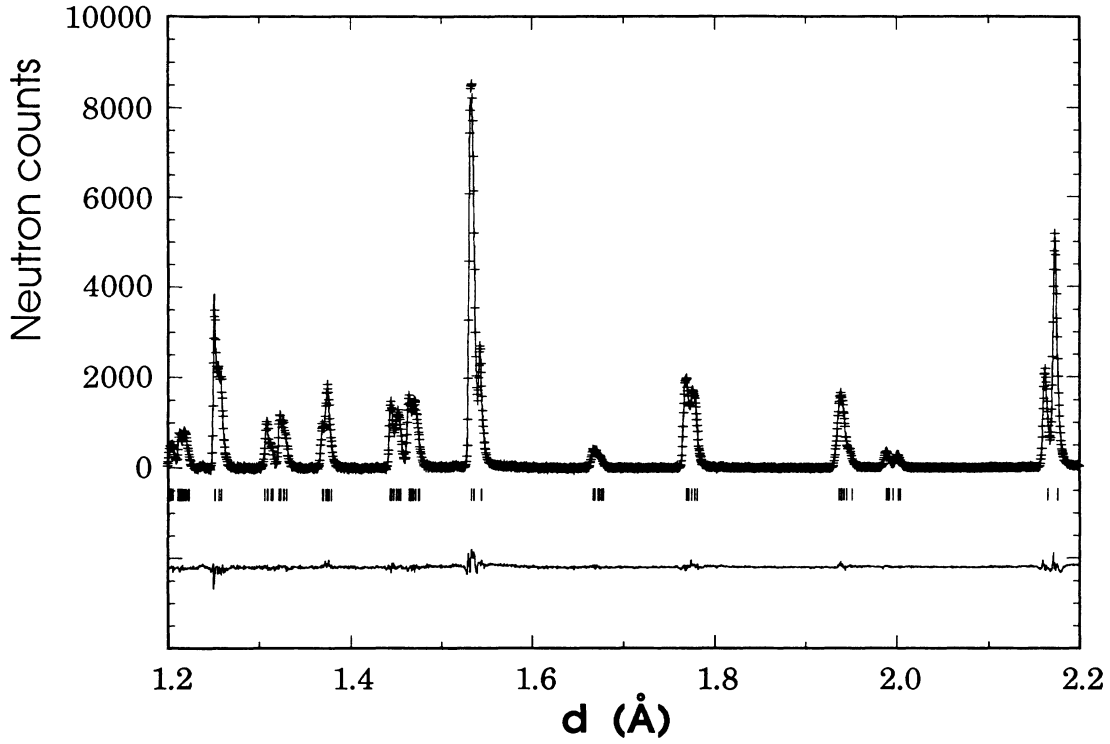

FIG. 2. Portion of the Rietveld refinement profile for $BaBi_{0.90}Pb_{0.10}BiO_3$ at 295 K based on a monoclinic, $I2/m$, refinement model. Plus marks (+) are the raw neutron-powder-diffraction data. The solid line is the calculated profile. Tick marks below the profile mark the positions of allowed Bragg peaks. A difference curve (observed minus calculated) is plotted at the bottom. Background was fitted as part of the refinement but has been subtracted prior to plotting.

versus composition is plotted in Fig. 3(a). β extrapolates smoothly to 90° near $x=0.23$. The average Bi—O bond lengths are plotted in Fig. 3(b). The bond length is taken as the average distance from a Bi(Pb) site to its six octahedrally coordinated oxygen neighbors. The average bond lengths for the two Bi sites, Bi(1)-O and Bi(2)-O, become equal between $x=0.20$ and $x=0.25$. For $x \geq 0.25$ the structure is orthorhombic, and there is only one Bi site per unit cell.

Within the resolution of our data for both the monoclinic angle, β, and the bond lengths, the transition from the monoclinic to the orthorhombic phase at room temperature is continuous and occurs near $x=0.23$, not at $x=0.10$ as previously reported.[1] Perhaps the reason for our different result is associated with the much higher instrumental resolution available on the General Purpose Powder Diffractometer. Lead substitution on the bismuth site is less effective in destroying the CDW associated with the two bismuth sites in the $BaBiO_3$ monoclinic phase than potassium substitution on the barium site. In the $Ba_{1-x}K_xBiO_3$ system, at room temperature, the transition from monoclinic to orthorhombic symmetry occurs near $x=0.1$.[4] The orthorhombic *Ibmm* structure shown in Fig. 4 is observed for $0.25 \leq x \leq 0.65$. The *Ibmm* space group has the same rotation of BiO_6 octahedra around the pseudocubic [110] axis as the parent monoclinic structure of $BaBiO_3$ but does not have the breathing mode distortion around the bismuth atoms.[11]

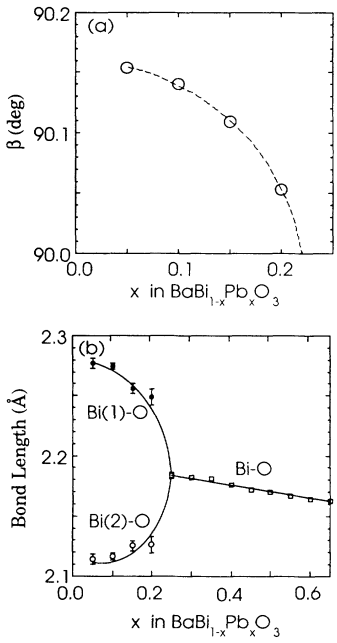

FIG. 3. (a) The monoclinic angle, β, and (b) the average Bi—O bonds lengths vs x for the monoclinic $I2/m$ phase of $BaBi_{1-x}Pb_xO_3$. The open square symbols [in (b)] show the average Bi—O bond length in the adjacent orthorhombic *Ibmm* phase. These results locate the monoclinic-to-orthorhombic transition near $x=0.23$.

Thus, there is one bismuth site per unit cell. This is the same structure observed in $Ba_{1-x}K_xBiO_3$ when the breathing-mode distortion associated with the monoclinic $BaBiO_3$ parent phase disappears with increasing potassium content.[4] Figure 5 shows the Rietveld refinement

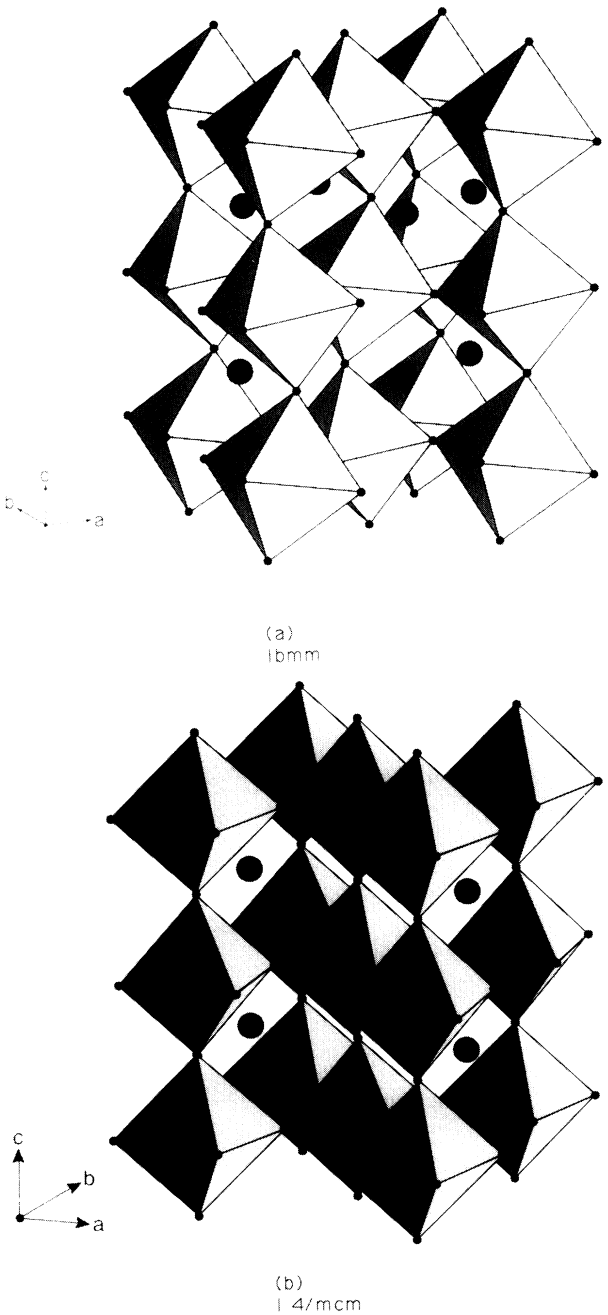

FIG. 4. Orthorhombic, *Ibmm*, and tetragonal, *I4/mcm*, distorted perovskite structures in the $BaBi_{1-x}Pb_xO_3$ system. The Ba atoms are shown as large filled circles; the oxygen atoms are represented as small filled circles; and the Bi(Pb) atoms (not shown) are located at the centers of the octahedra. Both structures are based on the simple cubic perovskite structure. In the orthorhombic structure (a) the Bi(Pb)-O octahedra tilt around the pseudocubic (110) axis. In the tetragonal structure (b) the octahedra tilt around the pseudocubic (010) axis.

TABLE II. Refined structural parameters for $BaBi_{1-x}Pb_xO_3$ at 295 K for the values of x listed. Space group: orthorhombic, *Ibmm* (No. 74). Numbers in parentheses are standard deviations of the last significant digit.

Parameter		$x=0.25$	$x=0.30$	$x=0.35$	$x=0.40$	$x=0.45$	$x=0.50$	$x=0.55$	$x=0.60$	$x=0.65$
a (Å)		6.1503(2)	6.1472(1)	6.1430(1)	6.1318(1)	6.1236(1)	6.1181(1)	6.1117(1)	6.1053(1)	6.1005(1)
b (Å)		6.1115(2)	6.1096(1)	6.1033(1)	6.1005(1)	6.0934(1)	6.0892(1)	6.0754(1)	6.0713(1)	6.0679(1)
c (Å)		8.6297(2)	8.6260(1)	8.6182(1)	8.6036(1)	8.5976(1)	8.5976(1)	8.5866(1)	8.5792(1)	8.5727(1)
Ba	x	0.4958(3)	0.4977(6)	0.4975(5)	0.4982(5)	0.4986(6)	0.4995(5)	0.4996(7)	0.5000(6)	0.501(7)
	B (Å^2)	0.89(3)	0.87(2)	0.92(2)	0.94(2)	0.86(2)	0.87(2)	0.77(2)	0.75(2)	0.80(2)
Bi(Pb)	B (Å^2)	0.35(2)	0.33(2)	0.38(1)	0.43(1)	0.39(2)	0.36(1)	0.31(2)	0.30(1)	0.30(2)
O(1)	x	0.0575(2)	0.0582(4)	0.0540(3)	0.0521(3)	0.0506(4)	0.0503(4)	0.0494(4)	0.0483(4)	0.0457(4)
	B (Å^2)	1.24(6)	1.20(4)	1.28(4)	1.34(3)	1.24(4)	1.21(3)	1.02(4)	1.01(2)	1.08(4)
O(2)	z	0.9709(2)	0.9707(2)	0.9713(2)	0.9722(1)	0.9729(2)	0.9737(1)	0.9748(2)	0.9755(2)	0.9758(2)
	B (Å^2)	1.56(5)	1.57(3)	1.59(3)	1.61(3)	1.50(3)	1.44(3)	1.27(3)	1.22(3)	1.25(3)
R_{wp} (%)		8.9881	6.9099	6.9786	7.4371	7.7171	7.3971	7.3972	6.7885	6.6665
R_{expt} (%)		5.3778	3.1958	3.4600	5.4990	5.7029	5.5483	4.2970	2.9264	3.2598
R_{wp}/R_{expt}		1.6714	2.1662	2.0170	1.3524	1.3532	1.3329	1.7215	2.3197	2.0451

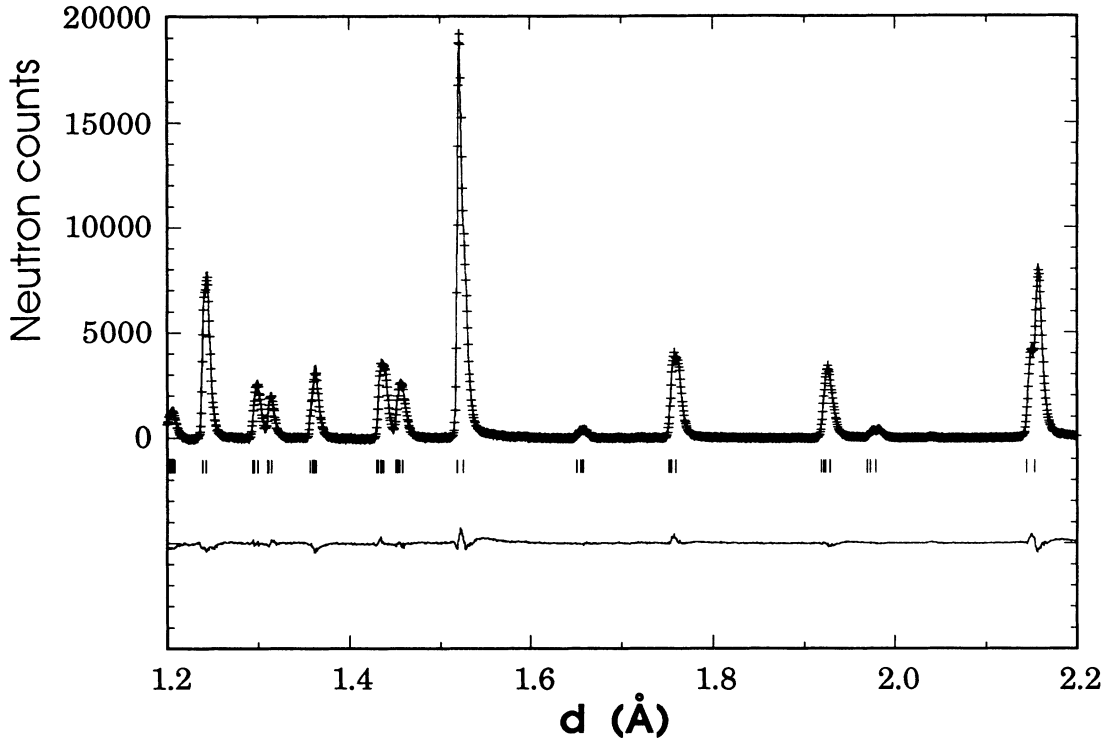

FIG. 5. Portion of the Rietveld refinement profile for $BaBi_{0.35}Pb_{0.65}BiO_3$ at 295 K based on an orthorhombic, *Ibmm*, refinement model. Format is the same as Fig. 2.

profile for the sample with $x=0.65$. Table II presents the refined orthorhombic structural parameters for samples with $0.25 \leq x \leq 0.65$. In the orthorhombic structure, the Bi—O bond lengths gradually decrease with increasing x for $0.25 \leq x \leq 0.65$ as shown in Fig. 3(b).

The neutron-powder-diffraction data for the samples with $0.70 \leq x \leq 0.80$ are not consistent with either the previously proposed orthorhombic (*Ibmm*) (Ref. 11) or tetragonal (*I4/mcm*) (Refs. 1 and 11) structures. Attempts to fit these data with single-phase orthorhombic or tetragonal models yielded obvious disagreements between the calculated and observed diffraction patterns for several Bragg peaks. Attempts to fit the data with the same monoclinic model as for $BaPbO_3$ were also unsuccessful. The observed diffraction patterns for $x=0.70$, 0.75, and 0.80 can be modeled as a mixture of orthorhombic and tetragonal phases in agreement with the conclusion of Sleight and Cox.[14] For the two-phase refinement, a goodness-of-fit parameter, R_{wp}/R_{exp},[20] of 1.71 was obtained, in contrast to values of 2.36 and 3.26 for the single-phase orthorhombic and tetragonal refinements, respectively. Differences of this magnitude indicate that the two-phase model is strongly preferred over either single-phase model. We later (see Fig. 8) show a Rietveld refinement of data at 10 K where the differences between the two phases are even more pronounced.

Table III lists the refined structural parameters for the coexisting tetragonal and orthorhombic phases for $x=0.70$, 0.75, and 0.80 at 295 K. The excellent agreement between calculated and observed diffraction data for all three samples, as well as for data taken as a function of temperature (to be discussed later) and the systematic behavior of the structural parameters confirms the validity of the two-phase refinement model.

Figure 6 shows the refined lattice parameters for the composition range $0.00 \leq x \leq 0.80$ that includes monoclinic, orthorhombic, and two-phase regions. The lattice constants for both the orthorhombic and tetragonal phases decrease linearly with increasing lead content for all compositions including those within the two-phase region. This is a good indication that the phase separation does not result from a miscibility gap in the phase diagram. If the samples had separated into two compositions because of a miscibility gap, the lattice parameters would remain unchanged across the two-phase region and only the relative phase fractions would vary.

TEMPERATURE-DEPENDENT DIFFRACTION EXPERIMENTS

In an attempt to understand the diphasic behavior, diffraction data for quenched and slowly cooled samples with the compositions $x=0.70$, 0.75, and 0.80 were compared. The differences resulting from the different thermal histories are clearly visible in the raw data and can be readily quantified by Rietveld refinement (to be discussed in detail later). The quenched samples have a larger tetragonal phase fraction than the slowly cooled samples. The differences between quenched and slowly

TABLE III. Refined structural parameters for $BaBi_{1-x}Pb_xO_3$, $x=0.70$, 0.75, and 0.80 at 295 K, based on a two-phase refinement model. Space groups: tetragonal, *I4/mcm* (No. 140) and orthorhombic, *Ibmm* (No. 74. Numbers in parentheses are standard deviations of the last significant digit.

Parameter		$x=0.8$ Tetragonal phase	$x=0.8$ Orthorhombic phase	$x=0.75$ Tetragonal phase	$x=0.75$ Orthorhombic phase	$x=0.70$ Tetragonal phase	$x=0.70$ Orthorhombic phase
a (Å)		6.0459(1)	6.0800(2)	6.0513(1)	6.0890(2)	6.0576(3)	6.0920(1)
b (Å)			6.0514(2)		6.0584(2)		6.0645(1)
c (Å)		8.6073(2)	8.5473(4)	8.6173(2)	8.5568(4)	8.6182(5)	8.5636(2)
Phase (%)		76(1)	24(1)	70(1)	30(1)	27(1)	73(1)
Ba	x		0.501(1)		0.501(1)		0.500(1)
	B (Å^2)	0.97(7)	0.57(7)	0.82(2)	0.82(1)	0.72(1)	0.73(1)
Bi(Pb)	B (Å^2)	0.60(3)	0.14(2)	0.38(1)	0.38(1)	0.44(1)	0.44(1)
O(1)	x		0.0454(8)		0.0463(9)		0.0459(4)
	B (Å^2)	1.40(6)	0.64(7)	1.14(4)	1.13(3)	0.38(3)	0.88(3)
O(2)	x	0.2182(3)		0.2197(3)		0.2145(8)	
	z		0.9731(6)		0.9739(7)		0.9770(2)
	B (Å^2)	1.41(5)	0.85(7)	1.21(2)	1.21(2)	1.14(2)	1.14(2)
R_{wp} (%)		6.0822		6.2191		5.5664	
R_{expt} (%)		3.4326		3.5306		3.2641	

cooled samples are largest for $x=0.80$ and smallest for $x=0.70$.

The $x=0.80$ sample was studied at temperatures between 10 and 575 K on both heating and cooling using neutron powder diffraction. This composition was chosen because it contains the largest fraction of tetragonal phase at room temperature. The transition from a single tetragonal phase at high temperature to a mixture of tetragonal and orthorhombic phases at lower temperature can be seen in the raw data. Figure 7 shows the (220) and (004) diffraction peaks at five temperatures between 10 and 575 K. At 10 K, the orthorhombic (220) diffraction peak is clearly seen between the tetragonal (220) and (004) peaks. As the temperature is increased, the splitting of the (220) and (004) peaks decreases for both phases and it becomes difficult to resolve the two phases in the raw data above room temperature. At 475 K a single tetragonal phase, with the expected splitting of the (220) and (004) peaks, is observed. As the temperature is increased further, the splitting decreases further and these peaks become nearly degenerate for 575 K.

Rietveld refinement provides a more quantitative way to analyze the data and to establish the phase transition temperature and the properties of the two coexisting phases. The Rietveld refinement profile for the data taken at 10 K is shown in Fig. 8. The refined structural parameters for the coexisting tetragonal and orthorhombic phases at this temperature are given in Table IV. All of the data from 10 to 425 K can be fit with a two-phase model. At and above 450 K, Rietveld refinements based on a single tetragonal phase provide the best fit to the data. Thus, within the resolution of our experiment, the tetragonal-to-orthorhombic transition occurs between 425 and 450 K.

The refined lattice parameters and cell volume versus temperature are shown in Fig. 9 for the single-phase ($T \geq 450$ K) and two-phase ($T \leq 425$ K) temperature regions. The lattice parameters and cell volume vary smoothly with temperature for each of the two phases.

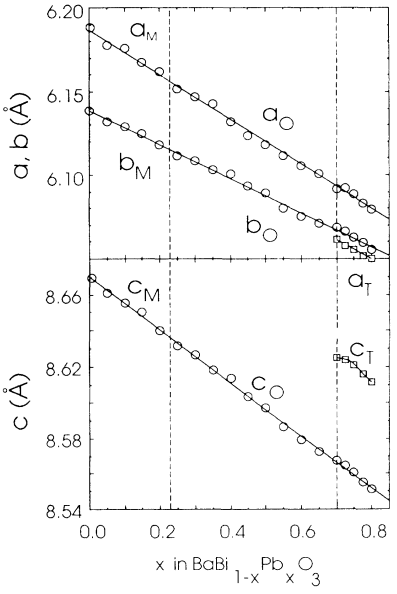

FIG. 6. Lattice parameters a, b, and c vs x for $BaBi_{1-x}Pb_xO_3$ as determined from Rietveld refinement using neutron-powder-diffraction data. Phase are identified by the subscripts M=monoclinic, O=orthorhombic, and T=tetragonal. In the region $0.70 \leq x \leq 0.80$, the parameters for both of the coexisting tetragonal and orthorhombic phases are shown.

TABLE IV. Refined structural parameters for $BaBi_{0.20}Pb_{0.80}O_3$ at 10 and 575 K. At 10 K tetragonal, *I4/mcm*, and orthorhombic, *Ibmm*, phases coexist. At 575 K, only the tetragonal, *I4/mcm*, phase is present. Numbers in parentheses are standard deviations at the last significant digit.

Parameter		$T=10$ K Tetragonal phase	$T=10$ K Orthorhombic phase	$T=575$ K Single-phase tetragonal
c (Å)		6.0217(1)	6.0767(3)	6.0726(2)
b (Å)			6.0328(3)	
c (Å)		8.6110(2)	8.5145(6)	8.6022(2)
Phase (%)		58(1)	42(1)	100
Ba	x		0.498(1)	
	B (Å^2)	0.20(2)	0.20(2)	1.42(2)
Bi(Pb)	B (Å^2)	0.055(11)	0.055(11)	0.61(2)
O(1)	x		0.513(9)	
	B (Å^2)	0.61(4)	0.61(4)	2.04(9)
O(2)	x	0.2134(3)		0.2306(2)
	z		0.9721(6)	
	B (Å^2)	0.45(2)	0.45(2)	2.23(4)
R_{wp} (%)			7.9496	7.8870
R_{expt} (%)			3.1255	3.5008

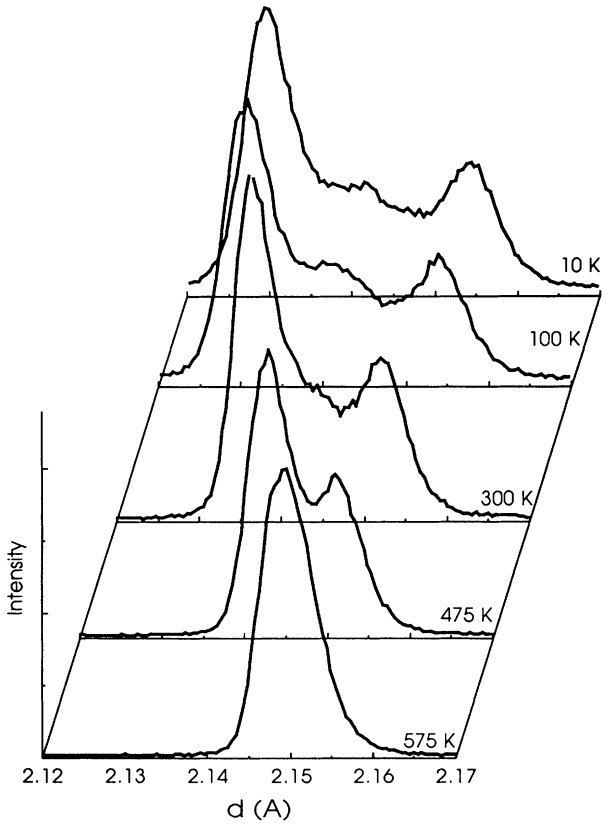

FIG. 7. Raw neutron-powder-diffraction data for $BaBi_{0.20}Pb_{0.80}O_3$ at several temperatures between 10 and 575 K. Above 450 K, the sample is single-phase tetragonal. Below 450 K, the sample is two-phase consisting of the tetragonal and orthorhombic phases.

Discontinuities in the lattice parameters at the transition temperature confirm that the transition is first order. However, no hysteretic behavior was observed. The plots include data taken on both heating and cooling. The decrease in the c axis and increases in the a and b axes of the orthorhombic structure at the phase transition temperature are consistent with the observation that the cell volumes of the two phase are nearly equal, as shown in Fig. 9(c).

The measured tilt angles for both phases are shown in Fig. 10. Over most of the temperature range where the tetragonal and orthorhombic phases coexist, the tilt angles are nearly equal. Thus, these two phases exhibit rotational distortions from the cubic perovskite structure of nearly equal magnitudes and differ only in the direction of the rotation axis. Near the transition temperature, the tilt angles diverge, with the tilt angle for the orthorhombic phase rapidly approaching zero. However, no anomaly is seen in the orthorhombic cell volume in this temperature range. This would require a distortion of the octahedra that preserves the cell volume while the tilt angle rapidly decreases. It is not clear whether this observation is real or whether the divergence in tilt angles results from correlations in the two-phase Rietveld refinements leading to incorrectly determined atom positions for the orthorhombic phase in the temperature range near the transition. One possible cause of such correlations could be the inability of the Rietveld model to fit enhanced diffraction line broadening (e.g., resulting from strain or small effective particle sizes) in the data for temperatures near the transition. The tilt angle for the tetragonal phase appears to smoothly approach zero as the temperature is increased toward 600 K, suggesting another phase

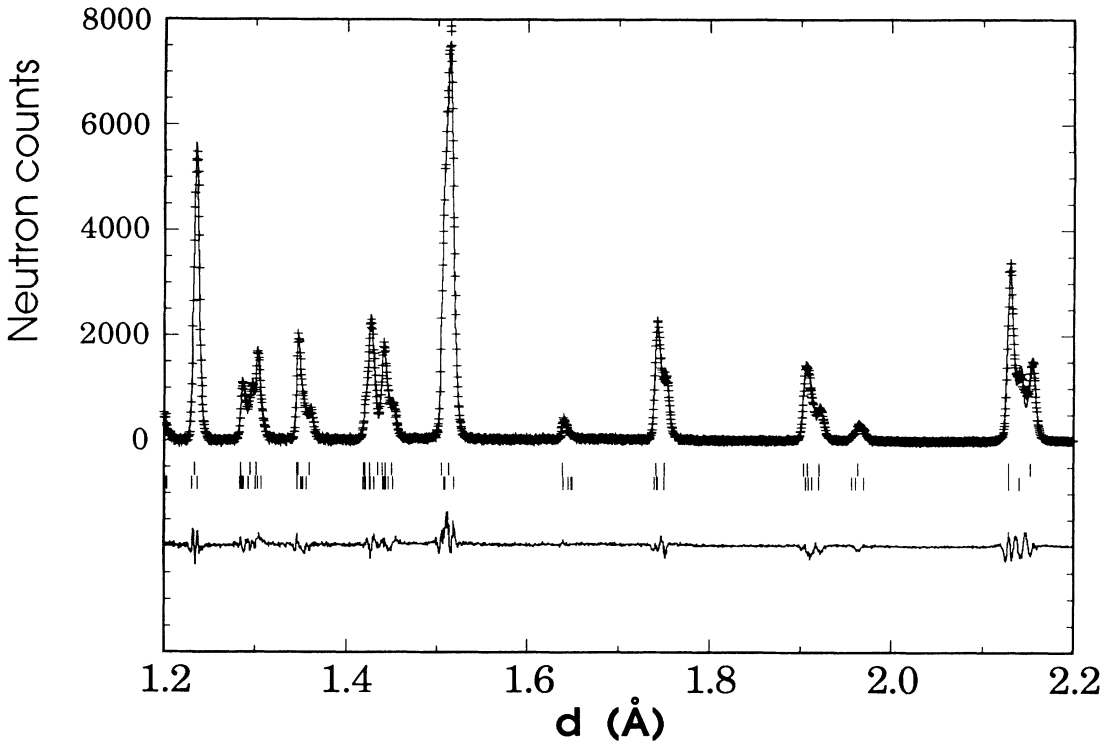

FIG. 8. Portion of the Rietveld refinement profile for $BaBi_{0.20}Pb_{0.80}BiO_3$ at 10 K based on a two-phase refinement including tetragonal, *I4/mcm*, and orthorhombic, *Ibmm*, phases. Format is the same as Fig. 2 except that upper tick marks are for the tetragonal peaks and lower tick marks are for the orthorhombic peaks.

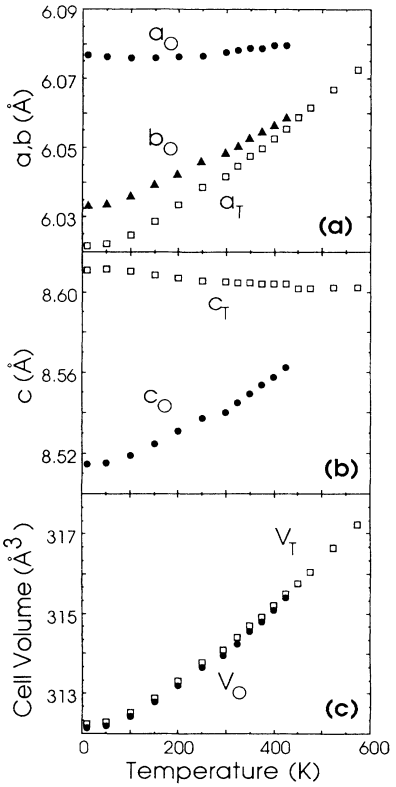

FIG. 9. Refined lattice parameters and unit-cell volumes vs temperature for the two phases present in $BaBi_{0.20}Pb_{0.80}O_3$. The open and filled symbols represent data for the tetragonal and orthorhombic phases, respectively.

transition (perhaps to a cubic phase) just beyond the temperature range of our experiments.

The volume fraction of the tetragonal phase, determined from the diffraction data by Rietveld refinement, versus temperature is shown in Fig. 11. The volume fraction falls from 100% at 450 K to about 60% at 250 K and then remains nearly constant at lower temperatures. Essentially the same phase fractions are observed on heating and cooling. Thus, the two-phase behavior can-

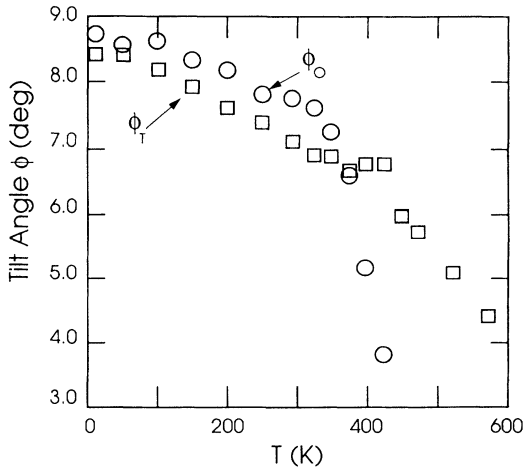

FIG. 10. Octahedral tilt angles for the two phases present in $BaBi_{0.20}Pb_{0.80}O_3$. The square and round symbols represent data for the tetragonal and orthorhombic phases, respectively.

not be attributed to hysteresis in the tetragonal-to-orthorhombic transition.

Our data provide no explanation for the two-phase behavior. However, similar behavior has been observed in other systems. Of these, the Chevrel-phase superconductors are especially interesting. In $SnMo_6S_8$ and $PbMo_6S_8$ a phase transition from the superconducting rhombohedral phase to an insulating triclinic phase begins above 100 K but is not complete at the onset temperature for superconductivity (14 K).[24,25] Thus, superconductivity is present only because a significant fraction of the metastable rhombohedral phase remains in the sample at 14 K. In $BaMo_6S_8$ the same transition begins at a much higher temperature (350 K) and is essentially complete at 100 K.[25] Thus, no superconductivity is observed in $BaMo_6S_8$ because the sample is entirely triclinic at low temperature. The onset temperature of the phase transition is systematically related to the size of the cation (Pb, Sn, Ba, etc.) and is quite sensitive to applied pressure. This behavior leads to a limit on the maximum T_c that can be achieved by changing the chemical composition.[25]

NORMAL STATE AND SUPERCONDUCTING PROPERTIES

Our measurements of the normal-state resistivities and the ac magnetic susceptibilities lead us to the conclusion that the tetragonal phase is metallic and superconducting and the orthorhombic phase is semiconducting. Figure 12 shows the dc resistivities for samples with $0.70 \leq x \leq 1.0$ prepared by slowly cooling. Samples with $0.80 \leq x \leq 1.0$ have a positive temperature coefficient of resistivity, $d\rho/dT$, indicating metallic behavior. Samples with $0.70 \leq x \leq 0.80$ show increasing resistive behavior with decreasing lead content. In fact, samples with $x = 0.70$ and 0.75 have $d\rho/dT < 0$, indicating nonmetallic behavior. Our diffraction measurements have shown that for samples with $x = 0.70$ and 0.75 the orthorhombic phase is the majority phase. This leads us to conclude

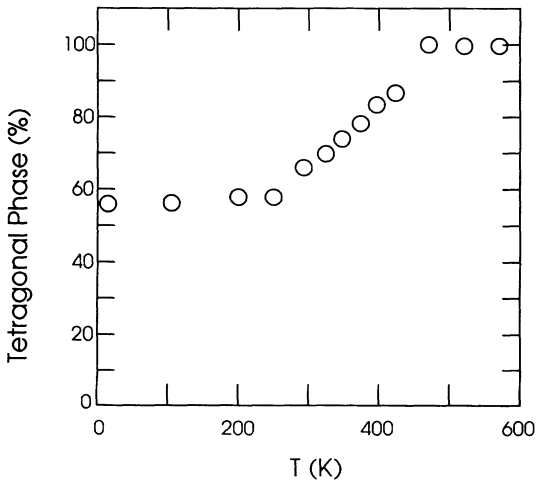

FIG. 11. Tetragonal phase fraction as a function of temperature for $BaBi_{0.20}Pb_{0.80}O_3$ as determined from Rietveld refinement using neutron-powder-diffraction data.

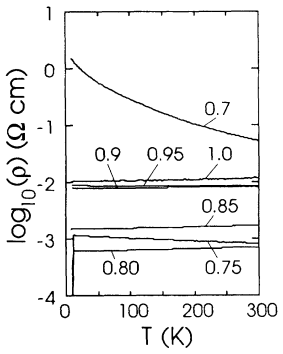

FIG. 12. dc resistivity data (plotted on a logarithmic scale) for $BaBi_{1-x}Pb_xO_3$ samples with $0.70 \leq x \leq 1.00$.

that the orthorhombic phase is semiconducting while the tetragonal phase is metallic, leading to the observed nonmetallic behavior for these diphasic samples. In support of these conclusions, we observe that the sample with $x = 0.80$ shows metallic conductivity and has the highest tetragonal phase fraction of the samples in this composition range.

Further evidence for the correlation between the tetragonal structure and superconductivity is obtained by comparing the results of ac susceptibility studies on the samples with $x = 0.70$, 0.725, 0.75, and 0.80 prepared either by quenching or by slowly cooling. Figure 13 shows the ac volume susceptibilities, $4\pi\chi$, versus temperature for these samples. The volume susceptibilities are calculated based on the theoretical densities with a value of $4\pi\chi = -1$ corresponding to full diamagnetism. For each composition, the quenched samples show a larger volume susceptibility and a sharper transition than the corresponding samples prepared by slow cooling. The susceptibilities at 5 K are plotted in Fig. 14 as a function of the tetragonal phase fractions obtained from the diffraction results. For all compositions, the superconducting phase fraction and tetragonal phase fraction are both larger for quenched samples than for slowly cooled samples. There is a clear trend for the superconducting phase fraction to increase as the tetragonal phase fraction increases, indicating that superconductivity occurs only in the tetragonal phase. The scatter of the data probably results from (1) the difficulty of determining an accurate superconducting phase fraction from ac susceptibility measurements; and (2) the inability of our ac susceptometer to reach temperatures below 5 K, giving only a lower limit to our superconducting phase fractions. We nevertheless conclude that only the tetragonal phase is superconducting. We also note that only a single superconducting transition is observed in each case. This observation contradicts the report by Oda *et al.*[10] that both phases are superconducting with different transition temperatures.

T_c VERSUS COMPOSITION FOR DOPED $BaBiO_3$ SUPERCONDUCTORS

To study the effect of doping on T_c further and allow for a direct comparison of the $BaBi_{1-x}Pb_xO_3$ and

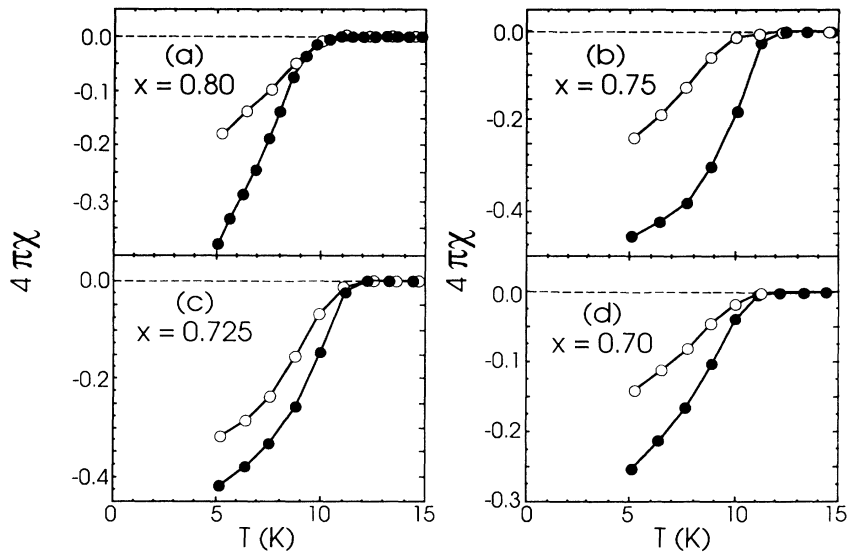

FIG. 13. ac susceptibilities vs temperature for quenched (filled symbols) and slowly cooled (open symbols) samples of $BaBi_{1-x}Pb_xO_3$ with $0.7 \leq x \leq 0.8$.

$Ba_{1-x}K_xBiO_3$ systems, several samples with compositions $Ba_{1-y}K_yBi_{1-x}Pb_xO_3$ were prepared. $BaCO_3$, Bi_2O_3, and PbO_2 in $1-y:1-x:x$ ratios were ball milled and fired in flowing oxygen at 800 °C for 8 h. The material was slowly cooled to room temperature and, subsequently, dry ball milled for 1 h. K_2O_2 was added to the Ba-Bi-Pb-O powder and the sample mixed inside a nitrogen-filled glove bag. The samples were placed into a gold boat and quickly transferred to a furnace tube with a 2% oxygen (in helium) gas flow. The samples were heated to 1000 K and held for 8 h before quenching to room temperature. The gas flow was then changed to high-purity oxygen without removing the sample from the furnace tube. To achieve full oxidation without potassium loss, the material was annealed at 700 K for 2 h, and then slowly cooled to room temperature.

Samples in the series $Ba_{1-y}K_yBi_{1-x}Pb_xO_3$ were studied using ac susceptibility measurements. The results for superconducting samples are summarized in Table V and plotted in Fig. 15 (cf. Hinks[26]). The circles represent the previous onset resistivity data for the $Ba_{1-x}K_xBiO_3$ system from Ref. 4. The squares are the transition onset temperatures taken from the ac susceptibility data presented in Fig. 13 for the quenched samples. The ac susceptibility data for the present $Ba_{1-y}K_yBi_{1-x}Pb_xO_3$ samples are shown as filled triangles. In the figure, the five triangles actually represent the results for eight superconducting samples, showing that samples with the same total dopant concentration, $x+y$, have the same T_c.

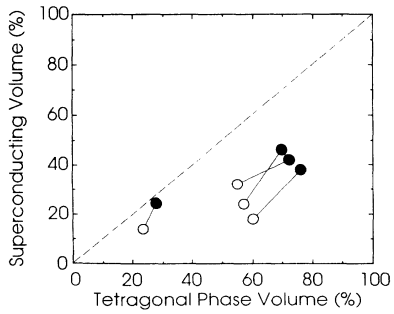

FIG. 14. Superconducting phase fractions (from ac susceptibility) vs tetragonal phase fractions (from neutron powder diffraction) for quenched (filled symbols) and slowly cooled (open symbols) samples of $BaBi_{1-x}Pb_xO_3$ with $x=0.70$, 0.725, 0.75, and 0.80. Lines connect the corresponding quenched and slowly cooled samples.

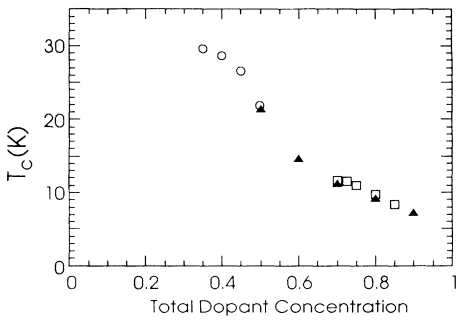

FIG. 15. Superconducting transition temperatures, T_c, vs total dopant concentration, $x+y$, for samples in the $Ba_{1-y}K_yBi_{1-x}Pb_xO_3$ system. The circles are the resistive onset temperatures taken from Ref. 4 for samples with potassium doping only ($x=0$). The squares (for $y=0$) and triangles (for $y\neq 0$ and $x\neq 0$) are from the present work and are onset data from ac susceptibility measurements. The five triangles represent data for eight samples of varying lead and potassium doping (since degenerate combinations of x and y are observed to produce the same T_c).

TABLE V. Superconducting transition temperatures, T_c, for $Ba_{1-y}K_yPb_{1-x}Bi_xO_3$ samples.

Total dopant concentration $x+y$	Lead content x	Potassium content, y	T_c
0.5	0.1	0.4	21.5
0.6	0.2	0.4	14.7
0.6	0.3	0.3	14.6
0.7	0.3	0.4	11.3
0.7	0.6	0.1	11.3
0.8	0.4	0.4	9.2
0.8	0.7	0.1	9.3
0.9	0.5	0.4	7.2
0.9	0.7	0.2	7.2

The $Ba_{1-y}K_yBi_{1-x}Pb_xO_3$ samples bridge the gap between the lead- and potassium-doped systems. T_c is an almost linear function of doping level, increasing as the half-filled band condition ($x=0$, $y=0$) is approached. For a given system, the maximum T_c occurs at a composition-dependent structural phase transition between an orthorhombic semiconducting phase and a metallic phase. The maximum T_c is limited by the structural instabilities that result in the opening of a gap at the Fermi energy. The lead-doped system is especially interesting in this regard since the superconducting tetragonal phase is itself metastable with respect to this transition. If the tetragonal-to-orthorhombic phase transition were complete, no superconductivity would be observed in the $BaBi_{1-x}Pb_xO_3$ system.

Further doping beyond that which gives the maximum T_c causes T_c to decrease. Although the T_c does not depend on the site of the doping, it is possible to stabilize a metallic phase at a doping level closer to the half-filled-band condition in the $Ba_{1-x}K_xBiO_3$ system, thus, allowing the higher T_c (30 K) to be obtained. These observations confirm the hypothesis of Mattheiss, Gyorgy, and Johnson,[15] who suggested that the higher T_c in the $Ba_{1-x}K_xBiO_3$ system is due to the doping concentration being closer to the half-filled band condition.

DISCUSSION AND CONCLUSIONS

The controversy in the literature concerning the room-temperature structures in the $BaBi_{1-x}Pb_xO_3$ system has been shown to be primarily the result of the existence of an incomplete structural transition from a high-temperature tetragonal phase to an orthorhombic phase. As a result, samples in the composition region $0.70 \leq x \leq 0.80$ are mixtures of the tetragonal and orthorhombic phases with the phase fractions depending somewhat on the rate of cooling from high temperature. Superconductivity is observed in samples within this same composition region. Using ac susceptibility data and Rietveld refinement of neutron-powder-diffraction data, we observe the superconducting volume fraction to generally increase with increasing tetragonal phase fraction and conclude that superconductivity only occurs in the metastable tetragonal phase.

The observed T_c in $Ba_{1-y}K_yBi_{1-x}Pb_xO_3$ compounds, where the structure and carrier concentration are modified by chemical substitution on both the barium and bismuth sites of $BaBiO_3$, is dependent on the ability to stabilize a superconducting phase at a dopant level as near as possible to the half-filled-band condition ($x=0$, $y=0$). T_c depends only on the total doping level, $x+y$, when a metallic-superconducting phase is stabilized.

ACKNOWLEDGMENTS

This work was supported by the U.S. Department of Energy, Division of Basic Energy Sciences—Materials Sciences, under Contract No. W-31-109-ENG-38 (J.D.J., D.G.H., R.L.H.) and by the National Science Foundation, Science and Technology Center for Superconductivity, under Grant No. DMR 88-09854 (D.T.M, S.P., P.G.R.).

*Also at Department of Physics, Illinois Institue of Technology at the time of this work. Present address: Department of Physics, Southern Illinois University, Carbondale, IL 62901.

[1]D. E. Cox and A. W. Sleight, *Proceedings of the Conference on Neutron Scattering*, Gatlinburg, TN 1976, edited by R. M. Moon (National Technical Information Service, Springfield, VA 1976), p. 45.

[2]G. Thornton and A. J. Jacobson, Acta Crystallogr. Sec. B **34**, 351 (1978).

[3]C. Chaillout and J. P. Remeika, Solid State Commun. **56**, 833 (1985).

[4]S. Pei, J. D. Jorgensen, B. Dabrowski, D. G. Hinks, D. R. Richards, A. W. Mitchell, J. M. Newsam, S. K. Sinha, D. Vaknin, and A. J. Jacobson, Phys. Rev. B **41**, 4126 (1990).

[5]L. F. Mattheiss and D. R. Hamann, Phys. Rev. B **28**, 4227 (1983).

[6]Note that we have chosen to write the chemical formula as $BaBi_{1-x}Pb_xO_3$ rather than the commonly used formula $BaPb_{1-x}Bi_xO_3$ in order to emphasize the importance of viewing $BaBiO_3$ as the parent compound for both the lead- and potassium-substituted systems.

[7]A. W. Sleight, J. L. Gillson, and P. E. Bierstadt, Solid State Commun. **17**, 27 (1975).

[8]Y. Khan, K. Nahm, M. Rosenberg, and H. Willner, Phys. Status Solidi A **39**, 79 (1977).

[9]M. Oda, Y. Hadika, A. Katsui, and T. Murakami, Solid State Commun. **55**, 423 (1985).

[10]M. Oda, Y. Hadika, A. Katsui, and T. Murakami, Solid State Commun. **60**, 897 (1986); see also, Y. Enomoto, M. Oda, and T. Murakami, Phase Trans. **8**, 129 (1987).

[11]H. Asano, M. Oda, Y. Endoh, Y. Hidaka, F. Izumi, T. Ishigaki, K. Karahashi, T. Murakami, and N. Watanabe, Jpn. J. Appl. Phys. **27**, 1638 (1988).

[12]J. Ihringer, J. K. Maichle, W. Prandl, A. W. Hewat, and T. Wroblewski, Z. Phys. B **82**, 171 (1991).

[13]H. Ritter, J. Ihringer, J. K. Maichle, W. Prandl, A. Hoser, and A. W. Hewat, Z. Phys. B **75**, 297 (1989).

[14]A. W. Sleight and D. E. Cox, Solid State Commun. **58**, 347

(1986).
[15]L. G. Mattheiss, E. M. Gyorgy, and D. W. Johnson, Jr., Phys. Rev. B **37**, 3745 (1988).
[16]R. J. Cava, B. Batlogg, J. J. Krajewski, R. C. Farrow, L. W. Rupp, Jr., A. E. White, K. T. Short, W. F. Peck, Jr., and T. Kometani, Nature **332**, 814 (1988).
[17]D. G. Hinks, B. Dabrowski, J. D. Jorgensen, A. W. Mitchell, D. R. Richards, S. Pei, and D. Shi, Nature **333**, 836 (1988).
[18]D. G. Hinks, J. D. Jorgensen, D. R. Richards, B. Dabrowski, Y. Zheng, and S. Pei, Mol. Cryst. Liq. Cryst. **184**, 39 (1990); S. Pei, J. D. Jorgensen, D. G. Hinks, Y. Zheng, D. R. Richards, B. Dabrowski, and A. W. Mitchell, J. Solid State Chem. **95**, 29 (1991).
[19]J. D. Jorgensen, J. Faber, Jr., J. M. Carpenter, R. K. Crawford, J. R. Haumann, R. L. Hitterman, R. Kleb, G. E. Ostrowski, F. J. Rotella, and T. G. Worlton, J. Appl. Crystallogr. **22**, 321 (1989).
[20]R. B. Von Dreele, J. D. Jorgensen, and C. G. Windsor, J. Appl. Crystallogr. **15**, 581 (1982).
[21]D. E. Cox and A. W. Sleight, Solid State Commun. **19**, 969 (1976).
[22]D. E. Cox and A. W. Sleight, Acta Crystallogr. Sec. B **35**, 1 (1979).
[23]C. Chaillout, A. Santoro, J. P. Remeika, A. S. Cooper, G. P. Espinosa, and M. Marezio, Solid State Commun. **65**, 1363 (1988).
[24]J. D. Jorgensen and D. G. Hinks, Solid State Commun. **53**, 289 (1985).
[25]J. D. Jorgensen, D. G. Hinks, and G. P. Felcher, Phys. Rev. B **35**, 5365 (1987).
[26]D. G. Hinks, Mat. Res. Bull. **15**(6), 55 (1990).

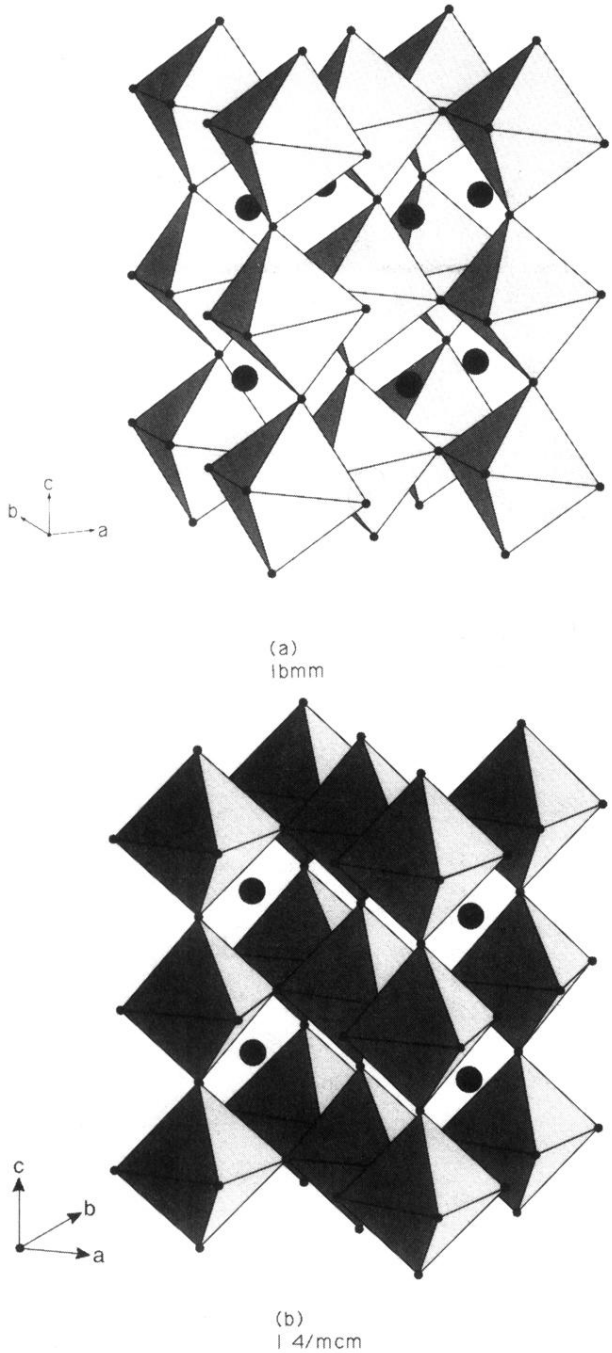

FIG. 4. Orthorhombic, *Ibmm*, and tetragonal, *I*4/*mcm*, distorted perovskite structures in the $BaBi_{1-x}Pb_xO_3$ system. The Ba atoms are shown as large filled circles; the oxygen atoms are represented as small filled circles; and the Bi(Pb) atoms (not shown) are located at the centers of the octahedra. Both structures are based on the simple cubic perovskite structure. In the orthorhombic structure (a) the Bi(Pb)-O octahedra tilt around the pseudocubic (110) axis. In the tetragonal structure (b) the octahedra tilt around the pseudocubic (010) axis.